

## Results of Predictive Fokker-Planck Modeling of Fusion Alpha Particles in ITER

V. Yavorskij<sup>1,2</sup>, V. Goloborod'ko<sup>1,2</sup>, L.G. Eriksson<sup>3</sup>, V. Kiptily<sup>4</sup>, K. Schoepf<sup>1</sup>,  
S.E. Sharapov<sup>4</sup>

<sup>1</sup>Association EURATOM-OEAW, Institute for Theoretical Physics, University of Innsbruck, Austria

<sup>2</sup>Institute for Nuclear Research, Ukrainian Academy of Sciences, Kiev, Ukraine

<sup>3</sup>Association EURATOM-CEA, CEA/DSM/DRFC, CEA-Cadarache, France

<sup>4</sup>EURATOM/UKAEA Fusion Association, Culham Science Centre, Abingdon, OX14 3DB, UK

### 1. Introduction

In comparison to the effect of charged fusion products (CFPs) in current tokamaks, CFPs in ITER are expected, due to the significantly enhanced fusion power, to have a stronger impact both on the plasma as well as on the first wall. Therefore the development of plasma scenarios and research programs for ITER requires a detailed kinetic modeling of fusion-born alphas. Here we present first results of predictive Fokker-Planck modeling of fusion alphas for basic ITER scenarios [1]. The main attention is paid to peculiarities of velocity and space distributions of confined alphas with energies exceeding 300 keV. The poloidal profiles of alpha density as well as of the fusion power deposition to electrons and ions are calculated. Also the alpha particle induced contributions to the bootstrap current and plasma rotation are evaluated. Finally we examine the energy spectra of lost alphas and present an assessment of the capabilities of diagnostics of confined fast alpha-particles in ITER.

### 2. Modelling results

The simulation carried out is based on the 3D COM Fokker-Planck approach previously used for modeling CFPs in JET [2, 3] and TFTR [4]. The modeling results

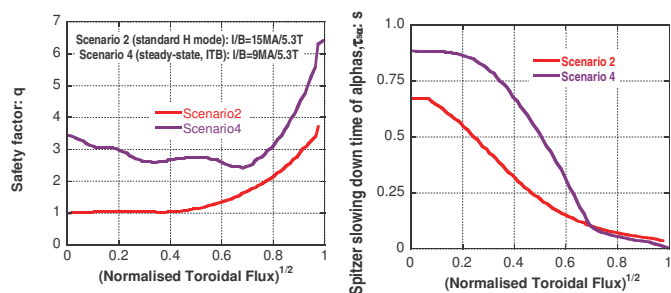


Fig. 1: The radial profiles of safety factor and Spitzer slowing-down time for the 2<sup>nd</sup> and 4<sup>th</sup> ITER scenario [1].

presented refer to ITER Scenario 2 (standard H-mode, I/B=15MA/5.3T) and to Scenario 4 (steady-state, ITB, I/B=9MA/5.3T). For these scenarios Fig. 1 displays the radial profiles of the respective safety factor  $q$  and the alpha Spitzer slowing-down time  $\tau_{\alpha}$ . Apparently, since the orbit width is proportional to  $q$ , wide orbit effects are more crucial for alpha transport in Scenario 4 as also is pitch angle scattering due to longer slowing-down times. This is confirmed by Fig. 2 which compares, for both scenarios, the modeled fusion alpha distribution functions  $f(R, V_{\parallel}/V, E, Z)$  for two energies ( $E=3.5\text{MeV}$ ,  $1.75\text{MeV}$ ) and  $Z$  taken at the plasma mid-plane. As expected due to the wider orbits, the initial distribution of alphas in the reversed shear plasma (Scenario 4) extends to a broader radial range and exhibits higher anisotropy in the longitudinal velocity  $V_{\parallel}$  than in the

standard 2<sup>nd</sup> Scenario. The anisotropy of alpha distributions is clearly seen from Figs. 2a, 2b where it becomes evident that co-going 3.5MeV alphas tend to aggregate at the low-B-field side, whereas counter-going alphas are displaced towards the high-B side. Again, due to the wider orbits, this displacement is more pronounced in the 4<sup>th</sup> Scenario. Figs 2c, 2d represent mid-plane distributions  $f(R, V_{||}/V)$  of partly thermalized alphas with  $E^*=1.75\text{MeV}$ . The finite-

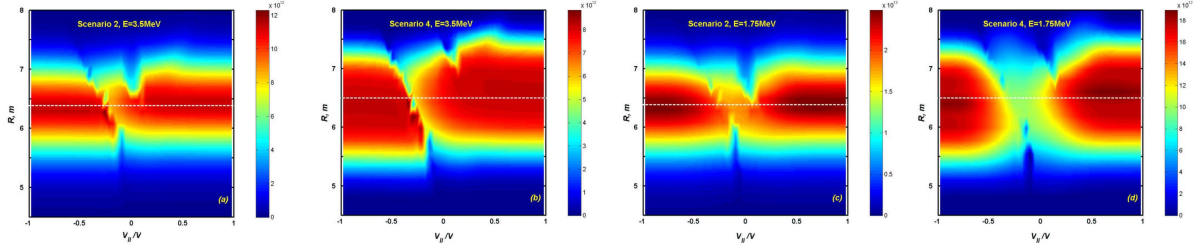


Fig. 2: Modeled distribution functions  $f(R, V_{||}/V, E^*, Z_{\text{mid-plane}})$  of fusion alphas for  $E^*=3.5\text{MeV}$  (plots a, b) and  $E^*=1.75\text{MeV}$  (plots c, d) for the 2<sup>nd</sup> and 4<sup>th</sup> ITER scenario. The distribution  $f$  is measured in particles per SI unit phase space volume.

orbits collisional transport considered here eventuates a redistribution of fast alphas both in the radial coordinate  $R$  as well as in the longitudinal energy. Due to the  $V_{||}$ -anisotropy in  $f(R, V_{||}/V, E, Z)$  the fusion alphas can generate a substantial longitudinal current  $j$  in the plasma. Fig. 3 displays the modeled  $R, Z$ -distribution of the density of the fusion alpha current in ITER plasmas for the 2<sup>nd</sup> and, respectively, the 4<sup>th</sup> Scenario. Due to the

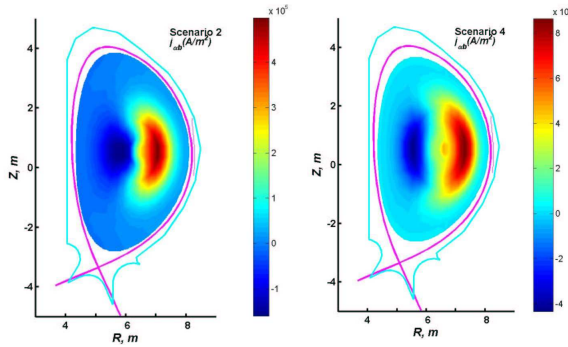


Fig. 3: Modeled  $R, Z$  profiles of the density of alpha current in  $\text{Am}^{-2}$  for the 2<sup>nd</sup> (left) and 4<sup>th</sup> ITER scenario (right).

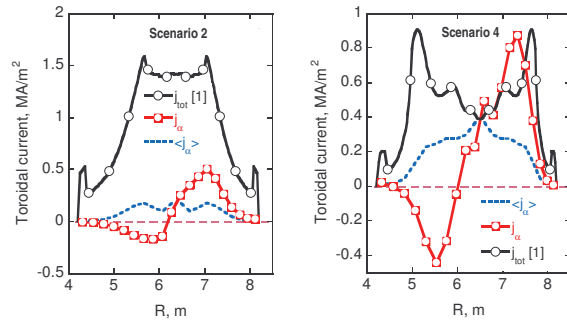


Fig. 4: Mid-plane profiles of the modeled density of alpha current and its flux surface average  $\langle j_{\alpha} \rangle$  for the 2<sup>nd</sup> (left) and 4<sup>th</sup> ITER scenario (right). Further indicated is the total plasma current density  $j_{\text{tot}}$  taken from [1] for the case of zero alpha density.

preponderance of co-going alphas on the low-B side and, conversely, of counter-going alphas on the high-B side the current  $j$  is, in the vicinity of the mid-plane, positive in the outboard plasma and negative in the inboard region. An important quantity for assessing how serious the plasma equilibrium is affected by fusion alphas, is the ratio of the alpha current  $j$  with respect to the total plasma current in the absence of DT fusion,  $j_{\text{tot}}$ . Figure 4 compares the mid-plane density profiles of the total plasma current with the alpha current and its average over the flux surface. It is seen that the alpha current can contribute significantly to the plasma current and, in the case of the 4<sup>th</sup> Scenario, it may even amount to a value comparable with  $j_{\text{tot}}$ . Note that the total alpha driven current  $j_{\alpha \text{tot}}$ , i.e. including that of alphas and also the reverse current of electrons following the alphas, is  $j_{\alpha \text{tot}} = \langle j_{\alpha} \rangle [1 - (1 - g) Z_{\alpha} / Z_{\text{eff}}]$  with  $g \sim (r/R)^{1/2}$  representing the trapped electron correction

to  $j_{\alpha tot}$  [5]. Thus the total alpha current may be substantially reduced by electrons. A noticeable impact on the plasma equilibrium is therefore possible only if  $\langle j_{\alpha} \rangle$  is large as is the case for the reversed shear plasma in Scenario 4. The reversed shear induced enhancement of  $j$  obtained here for the 4<sup>th</sup> Scenario is in agreement with the alpha current enlargement in the presence of a current hole in ITER, as resulted from Monte-Carlo modeling in [6, 7]. The plasma equilibrium is also influenced by the partial contribution of fusion alphas to the plasma pressure. In spite of the relatively low density of energetic alphas as compared to those of bulk plasma components ( $n_{\alpha} < 6.5 \cdot 10^{18} m^{-3} < 6\% n_e$  in Scenario 2 and  $n_{\alpha} < 4.5 \cdot 10^{18} m^{-3} < 6\% n_e$  in Scenario 4 as depicted in Fig. 5), the fast alpha contribution to the plasma beta can exceed 10% [1] attributable to the high energies of confined fusion alpha particles. Further of interest are the profiles of fusion power depositions to electrons and

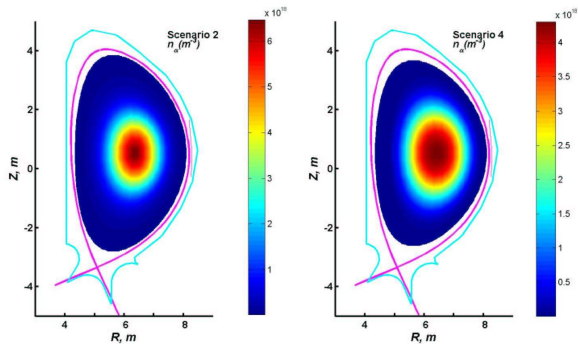


Fig. 5: Modeled R,Z-profiles of the density of fusion alphas ( $320keV < E < 3.5MeV$ ) in  $m^{-3}$  for the 2<sup>nd</sup> (left) and 4<sup>th</sup> ITER scenario (right)

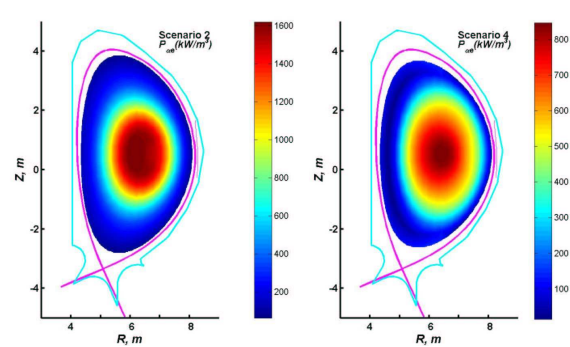


Fig. 6: Modeled R,Z-profiles of the fusion power deposited to electrons,  $P_{\alpha e}$ , in  $kWm^{-3}$  for the 2<sup>nd</sup> (left) and 4<sup>th</sup> ITER scenario (right)

ions,  $P_{\alpha e}$  and  $P_{\alpha i}$ , respectively. In Fig. 6 we present the poloidal profiles of  $P_{\alpha e}$  for the 2<sup>nd</sup> and 4<sup>th</sup> Scenario. Expectedly, due to the spatially extended alpha distribution in the reversed magnetic shear scenario #4, see Fig. 5, this scenario provides a broader region of fusion

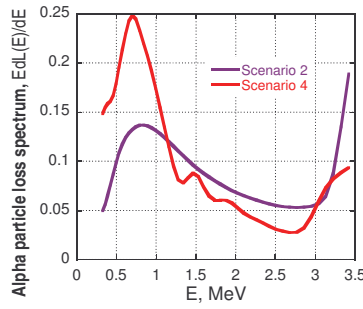
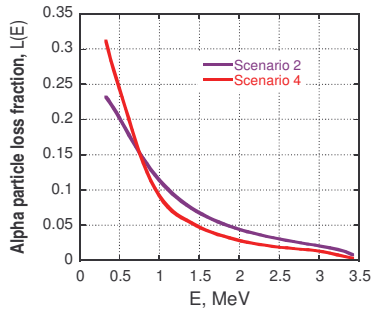


Fig. 7: Modeled alpha loss fraction (left) and energy spectra of lost alphas (right) for the 2<sup>nd</sup> and 4<sup>th</sup> ITER scenario

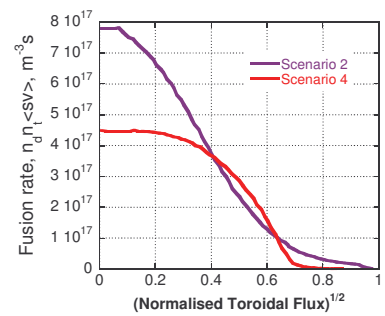


Fig. 8: Radial profiles of DT fusion rates for the 2<sup>nd</sup> and 4<sup>th</sup> ITER scenario

power deposition in Fig. 6 than the 2<sup>nd</sup> Scenario that exhibits the higher power density. For the plasma temperature around 25 keV assumed here, the alpha power transferred to bulk plasma ions is relatively small and corresponds to  $P_{\alpha d} < 20\% P_{\alpha e}$  and  $P_{\alpha t} < 15\% P_{\alpha e}$ .

To evaluate the fusion alpha impact on the first wall of ITER a predictive modeling of alpha loss distributions is needed. In ITER first orbit losses of alphas occur at a low level less than 10%, while collisional ripple transport (in the absence of ferritic inserts) constitutes the main loss mechanism. Neglecting first orbit losses, we display in Fig. 7 the fraction of fusion alphas lost at energies greater than the considered  $E$  and, further, the energy spectra of

these particles for the 2<sup>nd</sup> and 4<sup>th</sup> ITER Scenario. It is seen that alphas with energies in the ranges  $3\text{MeV} < E < 3.5\text{MeV}$  and  $0.5\text{MeV} < E < 1\text{MeV}$  contribute predominantly to the collisional losses. Note that for energies  $E > 1\text{MeV}$  alpha losses for the 2<sup>nd</sup> Scenario exceed those for the 4<sup>th</sup> Scenario, though the radial excursions of alphas are smaller in Scenario #2 than in #4. This is due to the diminutive fusion production at the plasma periphery ( $r > 0.7a$ ) in the 4<sup>th</sup> Scenario as shown in Fig. 8. However, the total collisional loss fraction of alphas in the entire energy range  $0.3\text{MeV} < E < 3.5\text{MeV}$  is about 31% in the 4<sup>th</sup> Scenario and exceeds the 24% loss fraction in the 2<sup>nd</sup> Scenario.

Finally, Fig. 9 demonstrates the mid-plane profiles of partly thermalized alphas with energies  $E > 1.8\text{MeV}$ , and further the profiles of  $\gamma$ -emission rates from  ${}^9\text{Be}(\alpha, n){}^{12}\text{C}$  reactions

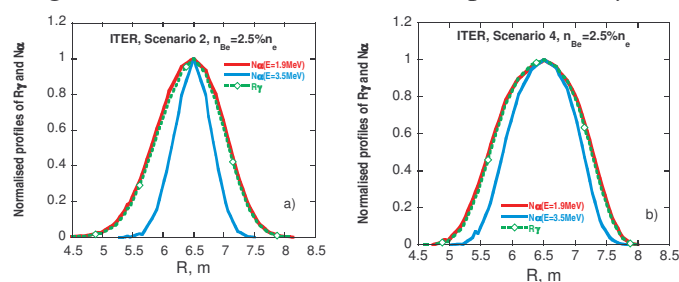


Fig. 9: Modeled profiles of the  $\gamma$ -emission rates from  ${}^9\text{Be}(\alpha, n){}^{12}\text{C}$  reactions, of the density of partly thermalized alphas  $N_\alpha(E > 1.8\text{MeV})$ , and of  $N_\alpha(E = 3.5\text{MeV})$  for the 2<sup>nd</sup> scenario (left) and 4<sup>th</sup> scenario (right).

induced by alphas with  $E > 1.7\text{MeV}$ . In both scenarios collisional transport results in essential broadening of the mid-plane profiles of partly thermalized alphas when compared to the initial profiles of alphas at birth energy. Notice that the  $\gamma$ -emission profiles are consistent with the density profiles of partly thermalized alphas, thus conforming the attractiveness of  $\gamma$ -diagnostics of energetic alphas.

### 3. Summary

Our predictive Fokker-Planck modeling of fusion alphas in ITER demonstrates a prominent sensitivity of alpha behaviour to plasma scenarios. A significant dissimilarity of alpha distributions over spatial coordinates and the longitudinal energy is observed for the 2<sup>nd</sup> and 4<sup>th</sup> ITER Scenario. Particularly the longitudinal anisotropy of alpha distributions in the 4<sup>th</sup> Scenario leads to a rather strong alpha current that is comparable to the total plasma current in the absence of fusions. The poloidal profiles of alpha density as well as of the fusion power deposition to electrons and ions extend to a broader region in Scenario #4 than in #2. Coulomb collisions result in a substantial (about 25-30%) loss of partly thermalized fusion alphas ( $E > 0.33\text{MeV}$ ) with the energy spectra of lost alphas seen to be sensitive to the plasma scenarios. Finally substantiated is the capability of  $\gamma$ -diagnostics of confined fast alpha-particles in ITER.

### Acknowledgement

This work has been partially carried out within the Association EURATOM-OEAW and under EFDA. The views and opinions expressed herein do not necessarily reflect those of the European Commission.

1. A.P. Polevoi et al., *J. Plasma Fusion Res. Series* **5**, 82 (2002).
2. V.A. Yavoskij, et al., *Nucl. Fusion* **43**, 1077 (2003).
3. K. Schoepf et al., *Kerntechnik* **67**, 285 (2002).
4. V.Ya. Goloborod'ko, et al., *Nucl. Fusion* **35**, 1523 (1995).
5. S.P.Hirshman, *Phys. Fluids* **31**, 3150 (1988).
6. M. Schneider, et al., *Phys. Plasmas Contr. Fus.* **47**, 2087 (2005)
7. A. Fasoli et al., *Nucl. Fusion* **47** S264–S284 (2007).